

Dual-wavelength digital holographic microscopy with sub-nanometer axial accuracy

Jonas Kühn^a, Florian Charrière^a, Tristan Colomb^b, Frédéric Montfort^c, Etienne Cuche^c, Yves Emery^c, Pierre Marquet^b and Christian Depeursinge^a

^aEcole polytechnique fédérale de Lausanne, Institute of imaging and applied optics, 1015 Lausanne, Switzerland;

^bCentre de Neurosciences Psychiatriques, Département de psychiatrie DP-CHUV, Site de Cery, 1008 Prilly-Lausanne, Switzerland;

^cLyncée Tec SA, PSE-A, 1015 Lausanne, Switzerland

ABSTRACT

We present dual-wavelength Digital Holographic Microscopy (DHM) measurements on a certified 8.9 nm high Chromium thin step sample and demonstrate sub-nanometer axial accuracy. We introduce a modified DHM Reference Calibrated Hologram (RCH) reconstruction algorithm taking into account amplitude contributions. By combining this with a temporal averaging procedure and a specific dual-wavelength DHM arrangement, it is shown that specimen topography can be measured with an accuracy, defined as the axial standard deviation, reduced to at least 0.9 nm. Indeed, it is reported that averaging each of the two wavefronts recorded with real-time dual-wavelength DHM can provide up to 30% spatial noise reduction for the given configuration, thanks to their non-correlated nature.

Keywords: Digital holography, phase imaging, optical metrology, non-contact, real-time

1. INTRODUCTION

Digital Holographic Microscopy (DHM) is a novel imaging technique that allows measuring quantitatively the wavefront transmitted through or reflected by a specimen seen through a Microscope Objective (MO) [1,2]. A hologram, namely the interference pattern between a wave coming from the object (the object wave) with a reference wave, is recorded with a digital camera and then digitally processed by computer to extract both the wavefront amplitude and phase information. As it is an interferometric method, DHM can provide so-called phase images with nanometer-range accuracy along the optical axis, revealing detailed information about the specimen topography or refractive index.

DHM is a well suited technique for optical metrology, e.g. for either micro-optics testing [3,4], MEMS-MOEMS characterization [5,6], microstructures investigation [7] or even roughness measurements [8]. The key advantages of DHM in this field are given by the remarkably high measurement stability and robustness of DHM, which results from the off-axis configuration allowing single hologram CCD acquisition for a very short duration integration period (down to few μs). Compared to phase-shifting interferometric techniques, DHM offers similar performance in terms of resolution, precision, repeatability, and field of view but can be considered as an attractive solution presenting specific and unique advantages over these methods: the acquisition rate is higher, because a complete reconstruction of the complex wavefront can be carried out out of a single hologram, and sensitivity to external vibrations is reduced since the acquisition time can be reduced down to a few tens of microseconds. Finally, DHM enables exclusively a so-called "digital focusing" by propagating digitally the complex wavefront, thus extending virtually the depth-of-field.

Different resolution enhancement techniques are presented in the present paper and topographic measurements are realized, with a dual-wavelength DHM setup on a 8.9 nm calibrated and certified step height. At

Further author information: (Send correspondence to Jonas Kühn)

E-mail: jonas.kuehn@a3.epf.ch, Telephone: +41 21 693 51 34

first, single-shot spatial standard deviations measurements on assumed-flat surfaces are obtained with a specific reference hologram reconstruction algorithm (see below), this for each individual wavelength. This reference hologram is acquired on a flat sample region due to FOV constrains. Secondly, the effect of temporal averaging on the reduction of the shot-noise contribution [9] is illustrated by considering again the spatial standard deviation values. Thirdly, the improvement of axial accuracy by dual-wavelength DHM is demonstrated by an averaging of both wavelengths topographic maps, reaching sub-nanometer accuracy. This dual wavelength averaging takes advantage of non-correlated noise between the two wavelengths used in the setup.

2. EXPERIMENTAL CONFIGURATION

The DHM setup used in this work allows imaging simultaneously at two different wavelengths. In previous works, this configuration was used to allow dual-wavelength DHM measurement with a single acquisition, in order to extend the phase dynamic range in the micrometer-range for configurations where unwrapping procedures fail to solve the phase ambiguity [10]. While the dual-wavelength approach has been already intensively applied in digital holography in a sequential way for nearly a decade [11–13], the method of Ref. [10] enables for the first time true real-time dual-wavelength imaging. Practically, this is achieved by subtracting two different wavelengths phase maps acquired during the same acquisition time to retrieve a so-called beat-wavelength phase image, the beat frequency being the frequency difference between both lasers, typically in the 5-20 μm range. As explained above, here another applications of the dual-wavelength operation mode is exposed, taking advantage of the non-correlation between these two available wavefronts. The optical arrangement is depicted in figure 1, with the laser sources consisting of two temperature-stabilized semiconductor laser diodes at $\lambda_1 = 657 \text{ nm}$ and $\lambda_2 = 680 \text{ nm}$. The diodes were tested for wavelength stability with a wavemeter and showed a wavelength deviation smaller than 10 pm over 8 h. The diodes also emit a low coherence (coherence length about 0.3 mm) linearly polarized light.

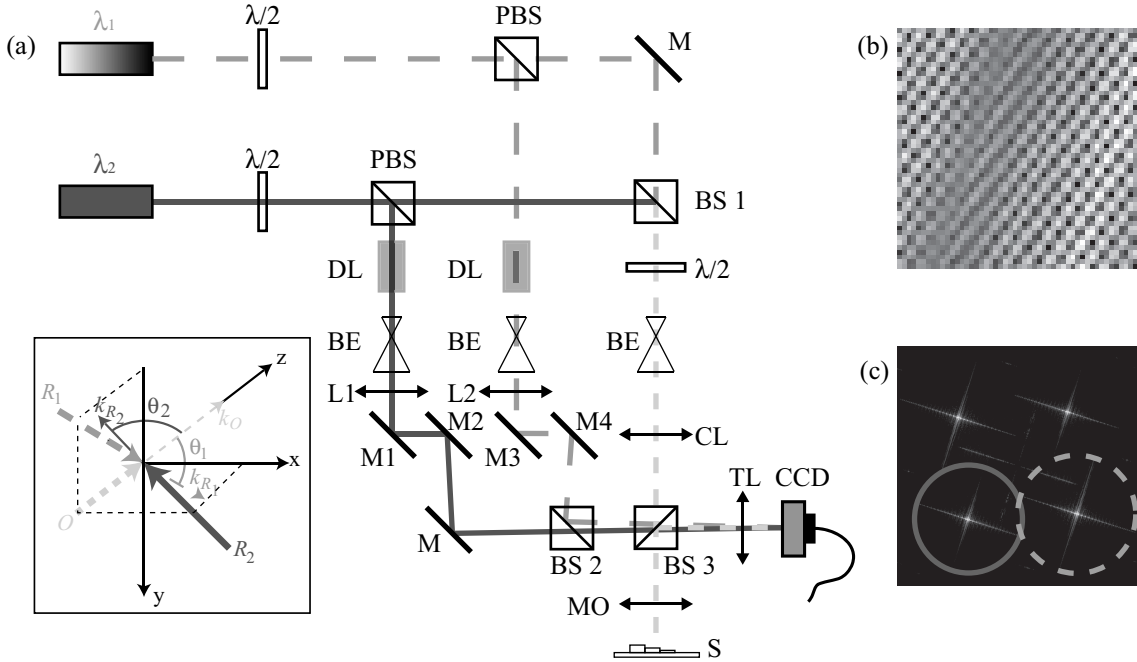


Figure 1. (a) Two-wavelengths DHM setup. $\lambda/2$: half-waveplates, M: mirrors, PBS: polarizing beamsplitters, BS: non-polarizing beamsplitters, DL: delay lines, BE: beam-expanders, L: lenses, CL: condenser lens, MO: x3 achromatic microscope objective, 0.1 NA, S: specimen, TL: tube lens; Inset: 3D distribution of the incident waves propagation directions upon the CCD plane, k_{R_1} and k_{R_2} are the propagation direction vector of the reference waves R_1 for wavelength λ_1 and R_2 for λ_2 ; (b) Zoom image of a part of the hologram, with the orthogonal fringe spatial frequencies; (c) Fourier spectrum of the hologram, where the wavefronts can be individually selected.

The main principle of the setup is to separate each wavelength beam pair in different reference arms, while aligning and combining them in an achromatic object arm. After reflection on the sample, both collinear object wavefronts are collected by the MO (infinity-corrected), and the object images are formed by the tube lens (focal 150 mm) about 50 mm behind the CCD plane. A low magnification x3 MO, with a NA of 0.1 (corresponding to $4.4 \mu\text{m}$ lateral resolution), is used in the present case to achieve large field-of-view (FOV), $1 \times 1 \text{ mm}^2$ with 512×512 pixels, and a large depth-of-field of more than $50 \mu\text{m}$. The CCD camera is a standard 8 bits black and white CCD camera with $6.45 \mu\text{m}$ pixel size. Each reference arm comprises a delay line (DL) adjusted to match the optical path length of the corresponding object beam, in order to create an interference on the CCD for both wavelengths. By tilting the pair of mirrors M1 and M2 for the first wavelength reference beam, respectively M3 and M4 for the second one, one can finely tune each k-vector incident upon the CCD camera. In other words, each wavelength interferograms fringes can be independently tuned both in spatial frequency and orientation.

The actual configuration is the one depicted in the inset of figure 1(a), with orthogonal spatial frequencies for each wavelength interferogram, because it ensures an optimum repartition of the interference terms in the hologram Fourier domain, minimizing overlaps.

The orthogonal repartition of the fringes spatial frequencies in figure 1(c) enables to filter (select) separately the spatial frequencies of each wavelength in the Fourier spectrum of the hologram [10]. This experimental configuration for recording holograms is very similar to the one in reference [14] and permits to encode both wavefronts with only a single acquisition thanks to orthogonal carrier frequencies. A transverse resolution of $4.4 \mu\text{m}$ has been measured with a USAF 1950 resolution test target and the system is diffraction-limited according to the NA of the MO.

The investigated sample is a thin step height standard from VLSI Standards Incorporated realized by Chromium deposition on a quartz wafer. It consists in a precisely etched positive step of $100 \mu\text{m}$ wide and $750 \mu\text{m}$ long, with a step height of 8.9 nm within a uncertainty of $\pm 0.5 \text{ nm}$, thus permitting measuring resolution-levels down to the nanometer. It is also important to notice that this test-target has been certified by the National Institute of Standards and Technology (NIST) to ensure correct measurements comparison with theoretical values. 3D-representations of this sample obtained from DHM reconstructed phase images presented later on in this paper are depicted in figure 2. All following measurements in this paper are related to the area of interest corresponding to figure 2(b).

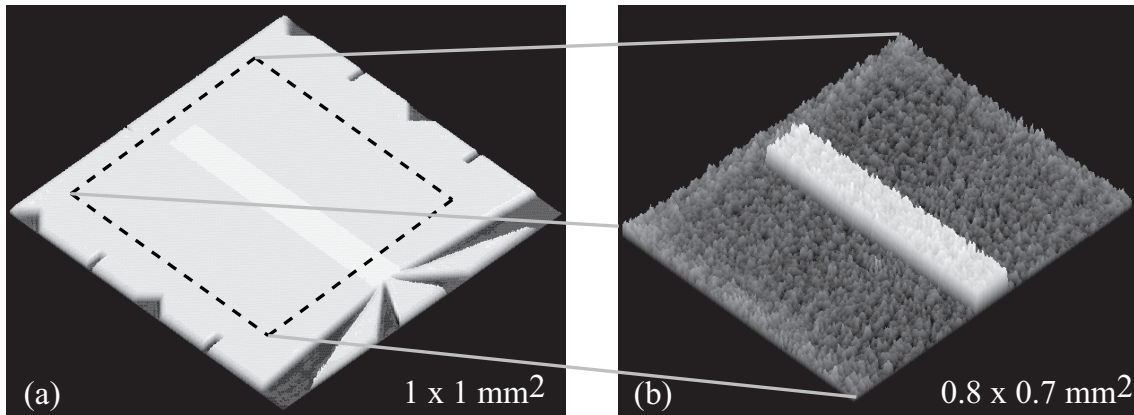


Figure 2. 3D-perspectives of the investigated thin step height standard obtained by the DHM setup of figure 1. (a) Full-FOV image with the surrounding structures pointing towards the calibrated 8.9 nm step; (b) Area of interest defined by the dashed rectangle in (a), where the considered step height is clearly visible.

3. REFERENCE-CALIBRATED HOLOGRAM RECONSTRUCTION ALGORITHM

Let us take the example of a hologram acquired by a digital camera, with two collinear object beams O_1 and O_2 at two different wavelengths λ_1 and λ_2 that interfere with two reference beams R_1 and R_2 , emitted by the same pair of laser sources, in a off-axis configuration (slight angle between object and reference beams). The intensity pattern, which results from an incoherent addition of both interferograms at λ_1 and λ_2 , can be expressed as

$$I_H(x, y) = |R_1|^2 + |O_1|^2 + |R_2|^2 + |O_2|^2 + R_1 O_1^* + R_1^* O_1 + R_2 O_2^* + R_2^* O_2, \quad (1)$$

with I_H being the hologram intensity, x, y the coordinates in the camera plane, and $*$ denoting the complex conjugate.

The first four terms in equation 1 correspond to the zero order of diffraction, and can be easily filtered out in the Fourier domain [15]. The last four terms correspond to the interference of the object wavefronts O_i (the virtual images), or their conjugate O_i^* (the real images), with the reference waves. These interferences appear as fringes with specific carrier spatial frequencies on the hologram. With O_i parallel to the optical axis, these carrier frequencies are dependent on the k-vectors of R_1 and R_2 . Considering different incident angles for the two references waves, especially the configuration where their k-vector projections on the CCD plane are orthogonal, each interference term occupies different positions in the Fourier plane. Provided that there is no overlap between interference terms, a condition which imposes restrictions regarding the spatial frequency content of the object spectrum, it is therefore straightforward to isolate each frequency component by spatial filtering [15]. Then it is possible to numerically propagate in a separate manner the two associated wavefronts. Such a procedure is completely identical to the one for real-time beat-wavelength DHM [10], and very similar to the arrangements for polarization imaging with digital holography [14]. Practically, the two different spatial filters allow to treat the two interference terms $R_1^* O_1$ and $R_2^* O_2$ independently.

Writing these two filtered holograms as $I_{H,1}^F$ for $R_1^* O_1$ and $I_{H,2}^F$ for $R_2^* O_2$ and by using the convolution formulation, we obtain the following expression for the Fresnel propagation:

$$\begin{aligned} \Psi_{CF,i}(m, n) = & \Gamma_i^I(m, n) \cdot \frac{\exp(i2\pi d_i/\lambda_i)}{i\lambda_i d_i} \cdot \\ & \text{FFT}^{-1} \left\{ \text{FFT} \left[\Gamma_{RCH_i}^H(k, l) I_{H,i}^F(k, l) \right] \cdot \right. \\ & \left. \exp \left\{ -i\pi\lambda_i d_i \left[\left(\frac{k}{N\Delta x} \right)^2 + \left(\frac{l}{N\Delta y} \right)^2 \right] \right\} \right\}, \end{aligned} \quad (2)$$

where $\Psi_{CF,i}$ is the reconstructed wavefront for wavelength λ_i in the convolution formulation, Γ_i^I is a digital phase mask (DPM) used to compensate for the tilt aberration in the image plane (see reference [16] for details), d_i is the propagation distance for wavelength λ_i , FFT is the Fast Fourier Transform operator, (k, l) and (m, n) are the couple of integers so that $(-N/2 < k, l, m, n \leq N/2)$ representing coordinates in the hologram plane, respectively the reconstruction plane, $N \times N$ is the number of pixels of the CCD camera and $\Delta x, \Delta y$ are the pixel sizes. $\Gamma_{RCH_i}^H$ is a so-called Reference Conjugated Hologram (RCH) used to compensate aberrations - directly in the hologram plane (without propagation) - with a calibration of the system (see below) defined as

$$\Gamma_{RCH_i}^H(k, l) = |R(k, l)|^{-1} |O_0(k, l)|^{-1} \exp[-i\varphi_0(k, l)] \quad (3)$$

where $|O_0(k, l)|$ is the amplitude of the object wave with an optical flat as specimen in the system (ideally modification of the object wavefront induced by the specimen), $\varphi_0(k, l)$ is the phase aberration function of the system during calibration and appear with a negative sign in equation 3 in order to cancel the system phase aberration in actual measurement.

The RCH technique was initially proposed by Colomb *et al.* [17]. It is similar to the double-exposure principle introduced by Ferraro *et al.* [18], but instead it operates directly in the hologram plane prior to propagation

and allows to compensate for phase aberrations and image distortion, by first recording a single calibration hologram, which is then used during the reconstruction process as in equation 2. Compared to the initial paper by Colomb *et al.*, the RCH defined here in equation 3 comprises also two amplitude terms $|R(k, l)|^{-1}$ and $|O_0(k, l)|^{-1}$, corresponding to the inverse of respectively the reference and the object wave amplitudes of the RCH. The insertion of these two amplitude terms in the definition of the RCH permits a full compensation of the amplitude inhomogeneities of the wavefront in the hologram plane. When not compensated, these amplitude inhomogeneities may transform in some phase aberrations after propagation of the wavefront to the image plane, especially in the low-frequency domain as illustrated in figure 3.

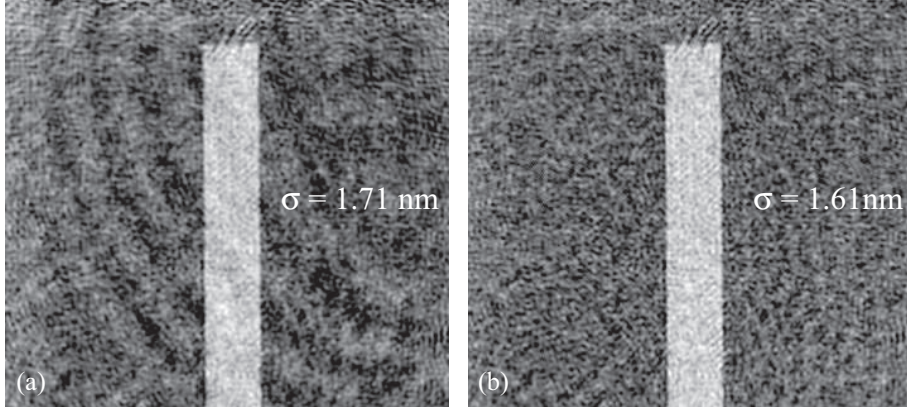


Figure 3. Comparisons between (a) the former DHM-reconstruction technique using the so-called Reference Conjugated Hologram (RCH) proposed by Colomb *et al.* [17] and (b) the modified RCH reconstruction technique presented in this paper incorporating amplitude correction. Both phase images of the VLSI Standards Incorporated test target comes from the same hologram recorded at a wavelength of 680 nm.

The formulation of equation 2 enables to propagate each wavefront $\Psi_{CF,i}$ in an independent manner: the DPM can be adapted to compensate for each individual wavefront tilt aberrations with respect to the reference hologram and the propagation distances d_i could be adjusted differently to compensate for slight chromatic aberrations or specimen displacement with respect to the working distance of the MO. The parallel propagations with 512x512 pixels holograms are achieved with a frame rate of about 7 frames per second with a standard dual-core PC at 2 GHz (roughly half the standard reconstruction rate). A a-posteriori hologram stack reconstruction can also be performed and a sequence recording becomes this way only limited by the acquisition rate of the CCD camera (here 25 frames per second).

4. RESULTS

4.1. Spatially-multiplexed single acquisition

In a first step, the two available wavefronts expressed in equation 2 are considered separately, and their corresponding phase images are reconstructed from a single hologram acquisition: this is quite similar to the standard mode of operation of single-wavelength DHM for real-time imaging at 15 frames/s with 512x512 pixels, apart from the simultaneous presence of two interferograms in the same frame, which are spatially multiplexed with orthogonal spatial frequencies (see Fig. 1). The reconstruction algorithm is the one of equation 2 with a single reference hologram acquisition, in another wafer area without structures, and the RCH approach with holograms amplitude division as presented in the previous section in equation 3. The dual-wavelength hologram and the reconstructed phases at both wavelengths are presented in figure 4.

The step height is directly measured in the phase images of figure 4(b,c), where the topographic spatial standard deviations are obtained as follows: $\sigma_1 = 1.93$ nm for $\lambda_1 = 657$ nm and $\sigma_2 = 1.62$ nm for $\lambda_2 = 680$ nm. These values are extracted by taking into account all the flat areas in the images FOV, the step itself and the surrounding substrate, and represent the usual parameter to estimate DHM axial accuracy. While these values are within the same 1.5-2 nm range, one can note that the image is a bit noisier for $\lambda_1 = 657$ nm than for λ_2

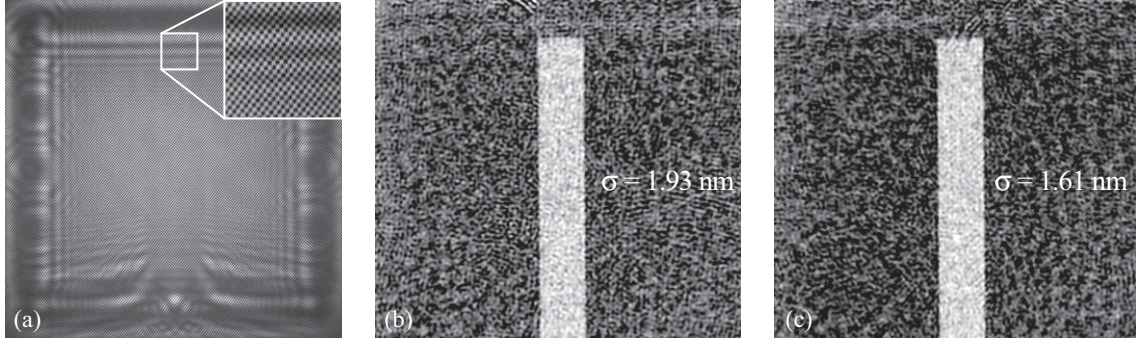


Figure 4. Reconstructed phase images at respectively (b) $\lambda_1 = 657$ nm and (c) $\lambda_2 = 680$ nm from the spatially-multiplexed dual-wavelength hologram of (a), with the zoom inset showing the orthogonal fringes spatial frequencies.

= 680 nm. This may be due by some wavelength- or source-dependency of the noise, either from remaining parasitic interferences, non-optimal Fourier filtering or signal-to-noise ratio differences due to degradation of the interference regimes (e.g. by linear polarization instability of the diodes).

4.2. Temporal wavefront averaging

As thoroughly explored in reference [9], shot noise contribution in DHM are not negligible, even in the current optical power configuration. Typically, with the red-range diodes used in this experiment and an integration time on the CCD camera of about 2 ms, the full electrons well capacity of the CCD chip ($16'000 e^-$ in our case) is easily reached, corresponding to an average of 8'000 photons per pixel over the whole hologram per frame acquisition [9]. However, due to the simultaneous acquisition of both interferograms, the available photons for one wavelength is only about 4'000 photons instead: in this regime the shot noise phase perturbation has a typical standard deviation between 0.25-0.6 degrees [9]. To attenuate this contribution to the phase noise, a temporal averaging over a 1 s period is applied by acquiring a sequence of 25 holograms at the maximum framerate of 25 images/s, then each reconstructed wavefronts in the hologram plane [19] are averaged, without individual propagation. This is done a first time for the reference hologram acquisition to obtain a "temporally-averaged reference hologram", then for the sample hologram with the temporally-averaged object wavefront in the hologram plane being digitally propagated at the end. The resulting phase images and spatial standard deviations for the step height specimen are illustrated in figure 5.

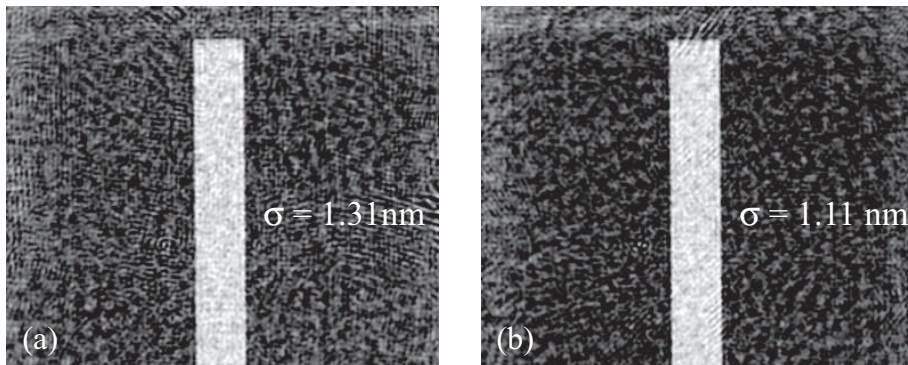


Figure 5. Temporal averaging over a 1s (25 holograms) sequence with the resulting phase image and spatial standard deviation at (a) $\lambda_1 = 657$ nm, (b) $\lambda_2 = 680$ nm.

By comparing the results with a 1 s temporal averaging of figure 5 with the single-shot measurements of figure 4, one can estimate the gain in axial precision as about 0.5-0.6 nm (0.5 degrees in phase) for the standard deviation, in this case corresponding to more than 30% enhancement. These values for the shot noise contribution

agree very well with the theoretical estimation given in reference [9] for the 4'000 photons regime under which the dual-wavelength DHM setup is operating. At this point, the nanometer-range axial precision is nearly reached.

4.3. Dual-wavelength wavefront averaging

The experimental configuration described in figure 1 provides two different wavefronts at different wavelengths during the same camera acquisition. This can be used to achieve a spatial averaging between both wavelength topographic maps obtained above. By making the hypothesis that these wavefronts are not correlated and follow a Gaussian noise distribution with similar topographic standard deviations σ_{xi} , one can write the following for the averaged topographic map standard deviation $\sigma_{\bar{x}}$:

$$\sigma_{\bar{x}} = \frac{\sqrt{2\sigma_{xi}^2}}{2} = \frac{\sqrt{2}}{2}\sigma_{xi} \quad (4)$$

From equation 4 it is clear that the spatial averaging process between both wavefronts is theoretically equivalent to a noise attenuation factor of $\frac{\sqrt{2}}{2}$, numerically a 0.71 multiplying factor or a -29% reduction. To validate this, Figure 6 presents the resulting spatially averaged topographic map obtained from the temporally averaged single-wavelength maps of Fig. 5.

The resulting spatial standard deviation in figure 6(c) is $\sigma = 0.87$ nm, thus achieving a sub-nanometer axial precision with DHM. Compared to the theoretical 30% gain of equation 4, the improvement is 28.5%, being in good agreement with the predicted value. This a-posteriori validates the hypothesis of uncorrelated wavefronts with two different laser sources at different wavelengths, and noise following a Gaussian relation. Qualitatively, this can also be observed by the "image granularity" reduction between figure 6(c,f) and figure 6(a,b,d,e).

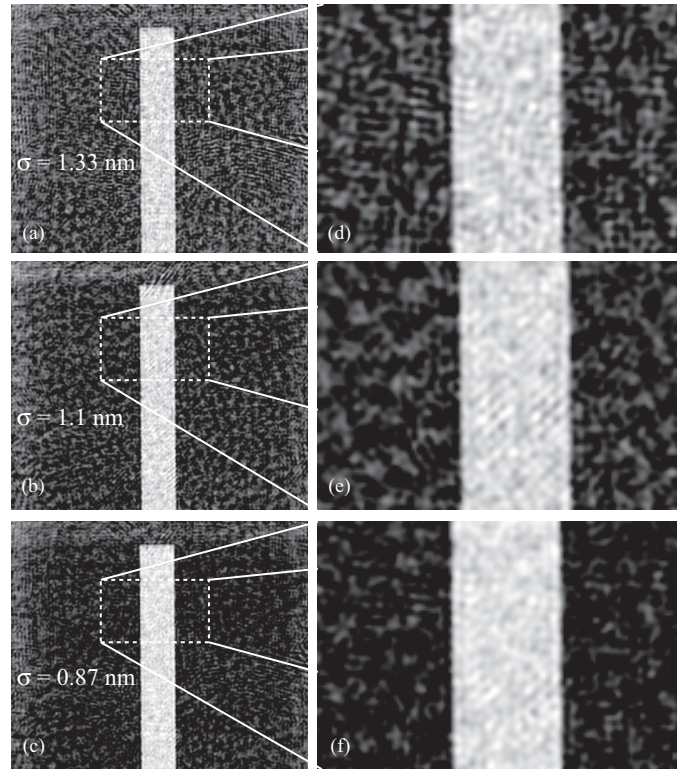


Figure 6. Topographic maps at (a) $\lambda_1 = 657$ nm, (b) $\lambda_2 = 680$ nm and (c) the resulting spatial average of (a) and (b), with (d,e,f) the corresponding zoomed area inside the white rectangles in (a,b,c).

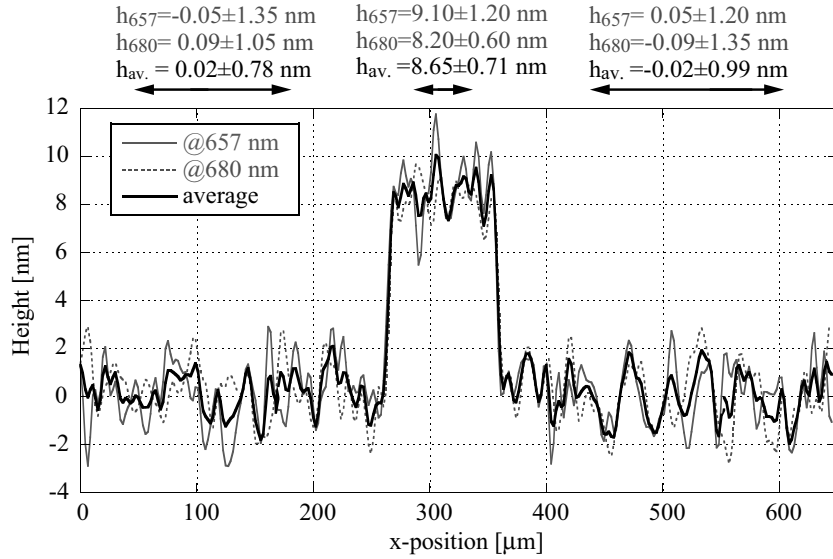


Figure 7. DHM profile measurement of the thin step height taken horizontally in figure 6 as a single median profile giving a Δh of 9.09 ± 1.27 nm, 8.20 ± 1.00 nm and 8.65 ± 0.83 nm for respectively λ_1 , λ_2 and the averaged result

Finally, figure 7 presents 1D profiles extracted out of figure 6 and gives measured heights in specific sections placed according to ISO-5436-1 standard. The profiles of figure 7 are obtained transversally along the horizontal median of figure 6(a-c). One can observe that when the noise standard deviation is too different between both wavelengths results, the relation of equation 4 is not valid any more: in this case the precision gain by averaging the wavefronts becomes negligible. Based on the measured heights in figure 7 the thin step can be estimated as 8.65 nm high, within the manufacturer uncertainty range. Moreover the standard deviation on flat areas reaching sub-nanometer values assess that this resolution level has been reached, given the sample certified roughness in the $-/+ 0.5$ nm range.

5. CONCLUSION

We presented Digital Holographic Microscopy (DHM) results with an axial topographic resolution reaching the sub-nanometer range. A 8.9 ± 0.5 nm high certified Chromium thin step sample was successfully investigated and measurements are within manufacturer uncertainty. To achieve sub-nanometric axial accuracy, three successive steps are necessary in this configuration. First, we expose a modified reference conjugated hologram (RCH) reconstruction algorithm capable of correcting amplitude-induced parasitic phase variations. Secondly, by temporal averaging of both reference and object holograms over a 1 s sequence it is possible to greatly reduce shot noise contributions, thus reducing noise by about 0.5 nm. Finally, we propose a novel single-acquisition dual-wavelength DHM approach to achieve wavefronts spatial averaging, leading to an additional 30% noise reduction gain and consequently enabling to break the nanometer barrier.

REFERENCES

1. E. CuChe, P. Marquet, and C. Depeursinge. Simultaneous amplitude-contrast and quantitative phase-contrast microscopy by numerical reconstruction of fresnel off-axis holograms. *Appl. Opt.*, 38(34):6994–7001, 1999.
2. U. Schnars and W. P. O. Juptner. Digital recording and numerical reconstruction of holograms. *Measurement Science and Technology*, 13(9):R85–R101, 2002.
3. Florian Charrière, Jonas Kühn, Tristan Colomb, Frédéric Montfort, Etienne CuChe, Yves Emery, Kenneth Weible, Pierre Marquet, and Christian Depeursinge. Characterization of microlenses by digital holographic microscopy. *Appl. Opt.*, 45(5):829–835, 2006.

4. J. Kühn, E. Cuche, Y. Emery, T. Colomb, F. Charrière, F. Montfort, M. Botkine, N. Aspert, and C. Depeursinge. Measurements of corner cubes microstructures by high-magnification digital holographic microscopy - art. no. 618804. In C. Gorecki, A. K. Asundi, and W. Osten, editors, *Optical Micro- and Nanometrology in Microsystems Technology*, volume 6188 of *Proceedings of the Society of Photo-Optical Instrumentation Engineers (Spie)*, pages 18804–18804, Bellingham, 2006. Spie-Int Society Optical Engineering.
5. F. Montfort, Y. Emery, F. Marquet, E. Cuche, N. Aspert, E. Solanas, A. Mehdaoui, A. Ionescu, and C. Depeursinge. Process engineering and failure analysis of mems and moems by digital holography microscopy (dhm). In *Proc. SPIE-Int. Soc. Opt. Eng.*, volume 6463 of *Reliability, Packaging, Testing, and Characterization of MEMS/MOEMS VI*, San Jose, CA, 2007.
6. G. Coppola, P. Ferraro, M. Iodice, S. De Nicola, A. Finizio, and S. Grilli. A digital holographic microscope for complete characterization of microelectromechanical systems. *Measurement Science and Technology*, 15(3):529–539, 2004.
7. S. De Nicola, P. Ferraro, A. Finizio, S. Grilli, L. Sansone, and P. De Natale. Two-dimensional characterization of relief microstructures in lithium niobate through digital holographic microscopy. In S. Demidenko, R. Ottoboni, D. Petri, V. Piuri, and D. C. T. Weng, editors, *Conference Record - IEEE Instrumentation and Measurement Technology Conference*, volume 2 of *Proceedings of the 21st IEEE Instrumentation and Measurement Technology Conference, IMTC/04*, pages 1344–1348, Como, 2004.
8. F. Montfort, Y. Emery, E. Solanas, E. Cuche, N. Aspert, P. Marquet, C. Joris, J. Kühn, and C. Depeursinge. Surface roughness parameters measurements by digital holographic microscopy (dhm). In *Proc. SPIE-Int. Soc. Opt. Eng.*, volume 6280 I of *Third International Symposium on Precision Mechanical Measurements*, Xinjiang, 2006.
9. Florian Charrière, Benjamin Rappaz, Jonas Kühn, Tristan Colomb, Pierre Marquet, and Christian Depeursinge. Influence of shot noise on phase measurement accuracy in digital holographic microscopy. *Opt. Express*, 15(14):8818–8831, 2007.
10. Jonas Kühn, Tristan Colomb, Frédéric Montfort, Florian Charrière, Yves Emery, Etienne Cuche, Pierre Marquet, and Christian Depeursinge. Real-time dual-wavelength digital holographic microscopy with a single hologram acquisition. *Opt. Express*, 15(12):7231–7242, 2007.
11. G. Pedrini, P. Froning, H. J. Tiziani, and M. E. Gusev. Pulsed digital holography for high-speed contouring that uses a two-wavelength method. *Appl. Opt.*, 38(16):3460–3467, 1999.
12. J. Gass, A. Dakoff, and M. K. Kim. Phase imaging without 2 pi ambiguity by multiwavelength digital holography. *Opt. Lett.*, 28(13):1141–1143, 2003.
13. Ichirou Yamaguchi, Takashi Ida, Masayuki Yokota, and Kouji Yamashita. Surface shape measurement by phase-shifting digital holography with wavelength shift. *Appl. Opt.*, 45(29):7610–7616, 2006.
14. Tristan Colomb, Florian Dürr, Etienne Cuche, Pierre Marquet, Hans Limberger, René-Paul Salathé, and Christian Depeursinge. Polarization microscopy by use of digital holography: application to optical fiber birefringence measurements. *Appl. Opt.*, 44(21):4461–4469, 2005.
15. E. Cuche, P. Marquet, and C. Depeursinge. Spatial filtering for zero-order and twin-image elimination in digital off-axis holography. *Appl. Opt.*, 39(23):4070–4075, 2000.
16. Tristan Colomb, Etienne Cuche, Florian Charrière, Jonas Kühn, Nicolas Aspert, Frédéric Montfort, Pierre Marquet, and Christian Depeursinge. Automatic procedure for aberration compensation in digital holographic microscopy and applications to specimen shape compensation. *Appl. Opt.*, 45(5):851–863, 2006.
17. Tristan Colomb, Jonas Kühn, Florian Charrière, Christian Depeursinge, Pierre Marquet, and Nicolas Aspert. Total aberrations compensation in digital holographic microscopy with a reference conjugated hologram. *Opt. Express*, 14(10):4300–4306, 2006.
18. P. Ferraro, S. De Nicola, A. Finizio, G. Coppola, S. Grilli, C. Magro, and G. Pierattini. Compensation of the inherent wave front curvature in digital holographic coherent microscopy for quantitative phase-contrast imaging. *Appl. Opt.*, 42(11):1938–1946, 2003.
19. Tristan Colomb, Frédéric Montfort, Jonas Kühn, Nicolas Aspert, Etienne Cuche, Anca Marian, Florian Charrière, Sébastien Bourquin, Pierre Marquet, and Christian Depeursinge. Numerical parametric lens for shifting, magnification and complete aberration compensation in digital holographic microscopy. *J. Opt. Soc. Am. A*, 23(12):3177–3190, 2006.